Bull. Mater. Sci., Vol. 35, No. 5, October 2012, pp. 853–858. © Indian Academy of Sciences.

Role of MgF_2 on properties of glass–ceramics

M GHASEMZADEH* and A NEMATI†

Department of Materials Engineering, Karaj Branch, Islamic Azad University, Karaj, Iran

†School of Materials Science and Engineering, Sharif University of Technology, Tehran, Iran

MS received 13 August 2011; revised 28 November 2011

Abstract. **Formation of machinable glass–ceramic in the system $MgO–SiO_2–Al_2O_3–K_2O–B_2O_3–F$ with and without addition of MgF_2 has been investigated. Crystallization of glass sample was done by controlled thermal heat treatment at nucleation and crystallization temperatures. The results showed that MgF_2 in high concentration had a synergistic effect and enhanced the formation of interlocked mica crystals. Non-isothermal DTA experiments showed that the crystallization activation energies of base glasses were changed in the range of 235–405 kJ/mol, while the crystallization activation energies of samples with addition of MgF_2 were changed in the range of 548–752 kJ/mol.**

Keywords. **Crystallization kinetics; glass ceramics; machinability; phlogopite.**

1. Introduction

Glass–ceramics have already found several applications as engineering materials and new uses constantly appear (Boccaccini 1997). The bulk chemical composition, nucleant added, final phase assemblage and microstructure are the most important factors affecting their technical properties. An important group of glass–ceramics is that of the mica-containing glass–ceramics, due to their high machinability, which results in an increased versatility of the products and numerous possibilities of industrial application (Baik *et al* 1997; Riello *et al* 2001; Taruta *et al* 2001).

Considerable research has been directed to mica glass–ceramic demonstrating excellent high temperature dimensional stability together with good machinability. Most naturally occurring micas have hydroxyl group in a silicate composition, whereas micas produced synthetically often involves fluorine substituted in the body structure in place of the hydroxyl groups. Thus, synthetic micas have frequently been termed as fluorophlogopite solid solutions or fluormicas. Investigation into the effect of fluorine on the properties of glasses have shown that it is network disruptive (Radonjic and Nikolic 1991; Likitvanichkul and Lacourse 1995; Greene *et al* 2003). The reduction in glass transition temperature of pre-cerammed cannasite glass–ceramics has been related to the creation of non-bridging fluorines which replace bridging oxygens in the glass network.

The purpose of this present work is to study the effect of variation of MgF_2 content on crystallization kinetics and microstructure of the prepared glass–ceramic.

2. Experimental

Reagent grade SiO_2, Al_2O_3, $MgCO_3$, MgF_2, K_2CO_3, TiO_2, H_3BO_3 powders were used. Homogeneous mixtures of batches (~100 g), obtained by ball milling, were melted in alumina crucibles at 1450°C in an electric kiln for 2 h. The resulting melt was quenched in preheated steel mould and immediately annealed at 500°C to eliminate stress. A portion of the frit was handmilled in an agate mortar to obtain glass powder for thermal analysis. Crystallization kinetics of glass powder was studied by differential scanning calorimetry (DSC) - DSC-1500 Rheometric scientific, USA calorimeter) with different heating rates (10, 15, 20 C/min). The crystallized phases of reheated samples were analysed by X-ray diffraction (XRD) (Philips PW 1800 X-ray diffractometer). After immersing in 10 wt% HF solution for 7–20 s, microstructures of reheated samples were analysed by SEM using Philips XL seines (XL30) electron microscope. Crystallized bulk samples were ground and polished. Vicker's hardness was performed with duramin microhardness tester with a pyramid-shaped diamond indenter (a load of 200 g for 30 s was applied). Cutting energy (μ^1) at quasi-static state is given by (Wang *et al* 2009).

$$\mu^1 = H_V^{2.25}. \tag{1}$$

Machinability parameter 'm' can be used to evaluate effects of heat treatments as a function of temperature, time and H_V (Wang *et al* 2009). Equation (2) indicates the relationship between hardness (H_V) and machinability parameter (m) (Wang *et al* 2009):

$$m = 0{\cdot}643 - 0{\cdot}122 H_V. \tag{2}$$

*Author for correspondence (ghasemzadeh@kiau.ac.ir)

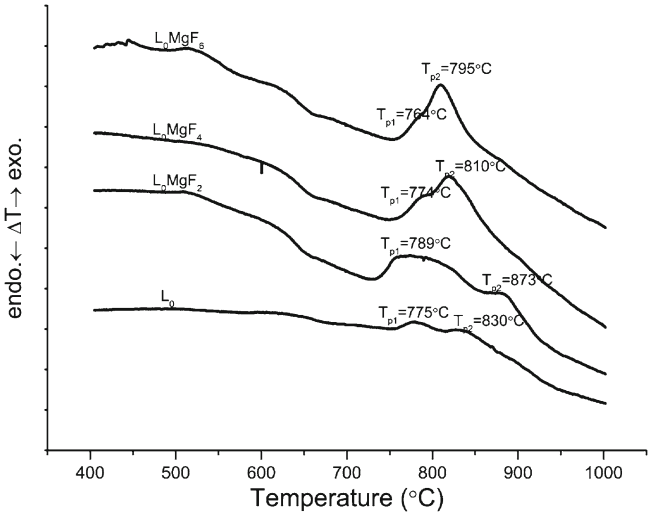

Figure 1. DTA patterns of glass samples.

Table 1. Results obtained from DTA curves of analysed samples.

Sample	T_g(°C)	T_p(°C)	$T = T_p - T_g$(°C)
L_0	634	775	141
L_0MgF_2	606	763	157
L_0MgF_4	620	780	160
L_0MgF_6	610	795	185

3. Results and discussion

3.1 *Theoretical basis*

Equation (3) has been used for crystallization evaluation, according to Kissinger's (1957) formula, which has been used to calculate the activation energy of crystallization, E_{ck}

$$\ln\left(\alpha/T_p^2\right) = \left(-E_{ck}/RT_p\right) + \text{constant}. \quad (3)$$

By ploting the $\ln\left(\alpha/T_p^2\right)$ vs $1/T_p$, a straight line should be obtained, from which the slope can be applied to determine E_{ck}. Matusita and Sakka (1980) stated that Kissinger method is valid only when crystal growth occurs on a fixed number of nuclei. Incorrect values for the activation energy are obtained if a majority of the nuclei are formed during DTA measurement, due to the number of nuclei continuously varying with α. They have proposed a modified form of the Kissinger equation as given below:

$$\ln\left(\alpha^n/T_p^2\right) = \left(-mE_c/RT_p\right) + \text{constant}, \quad (4)$$

where E_c is the correct or modified activation energy for crystallization and m the dimensionality of growth, which can take values ranging from 1–3 ($m = 1$, 2 and 3) for one-, two- and three-dimensional growth, respectively. $m = n-1$ when nucleation occurs during DTA and the number of nuclei in the glass is inversely proportional to α. In addition, when surface crystallization predominates, $m = n = 1$

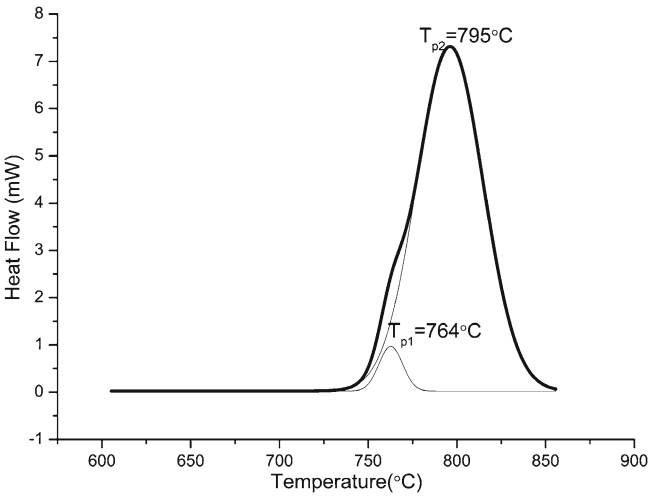

Figure 2. Separation of overlapped crystallized peaks for L_0MgF_6 ($\alpha = 10$ K/min).

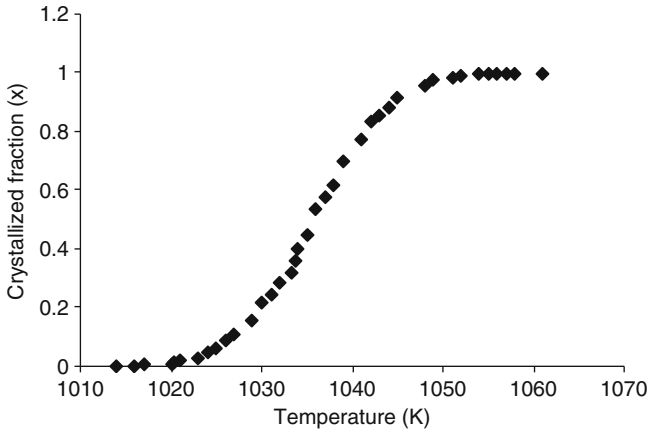

Figure 3. Crystallized fraction as a function of temperature for L_0MgF_6.

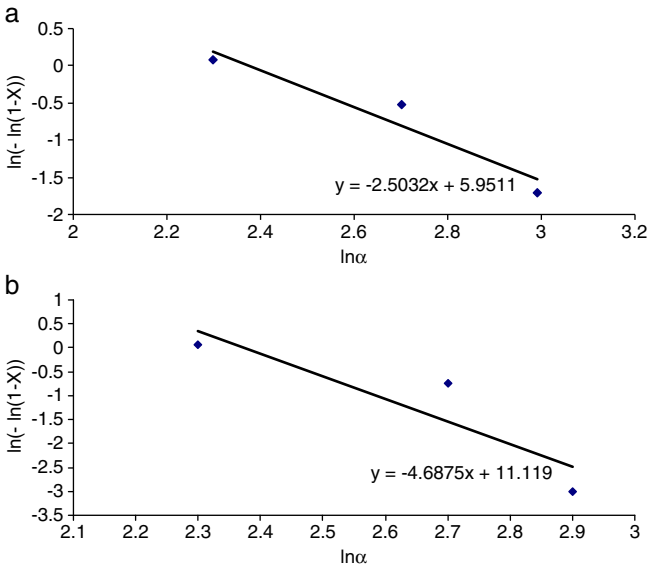

Figure 4. Plot of $\ln(-\ln(1-x))$ vs $\ln\alpha$ for (**a**) L_0 and (**b**) L_0MgF_6.

and (4) essentially reduces to the Kissinger equation. In other words, $E_{ck} = E_c$.

The Avrami exponent, n, can be evaluated by the modified Ozawa (1971) equation using a multiple scan analysis technique: first volume fraction, 'x' is calculated at the same temperature from a number of crystallization exotherms under different heating rates by the ratio of partial area to the total area crystallization exotherm. After plotting $\ln[-\ln(1-x)]$ vs $\ln\alpha$, and if the data can be fitted to the linear function, then the slope of the function would be $-n$, i.e.

$$d\ln[-\ln(1-x)]/d\ln\alpha = -n. \quad (5)$$

3.2 *Thermal stability*

Figure 1 shows DSC curves of glass samples at a heating rate of 10°C/min. T_g, crystallization temperature, glass transition temperature, T_p and thermal stability index, $\Delta T = T_p - T_g$ are listed in table 1. The bigger the thermal stability index 'ΔT', the more stable the glass and less tendency of crystallization.

As it is clear from table 1, the addition of 2%wt MgF_2 (L_0MgF_2) causes 19°C decrease on T_g of base glass and 14°C increase on T_p. The addition of 4%wt MgF_2 (L_0MgF_4) showed little effect on T_p and caused 34°C decrease on T_g.

T_g of L_0MgF_6 sample with 6%wt MgF_2 was 34°C lower than that of L_0 sample. The crystallization temperature also decreased. According to the values of ΔT, the order of thermal stability of different glasses can be listed as follows:

$$L_0MgF_2, L_0MgF_4 > L_0MgF_6 > L_0.$$

3.3 *Crystallization kinetics*

Figure 2 shows overlapping of the crystallization curves for DTA scan at $\alpha = 10°C \cdot min^{-1}$. Figure 3 shows the fraction, x, crystallized at a given temperature, T and is given by $x = A_T/A$, where A is the total area of the exothermic between the temperature, T_i, where crystallization just begins and the temperature, T_f, where the crystallization is completed, and A_T the area between T_i and T_f (Arora *et al*

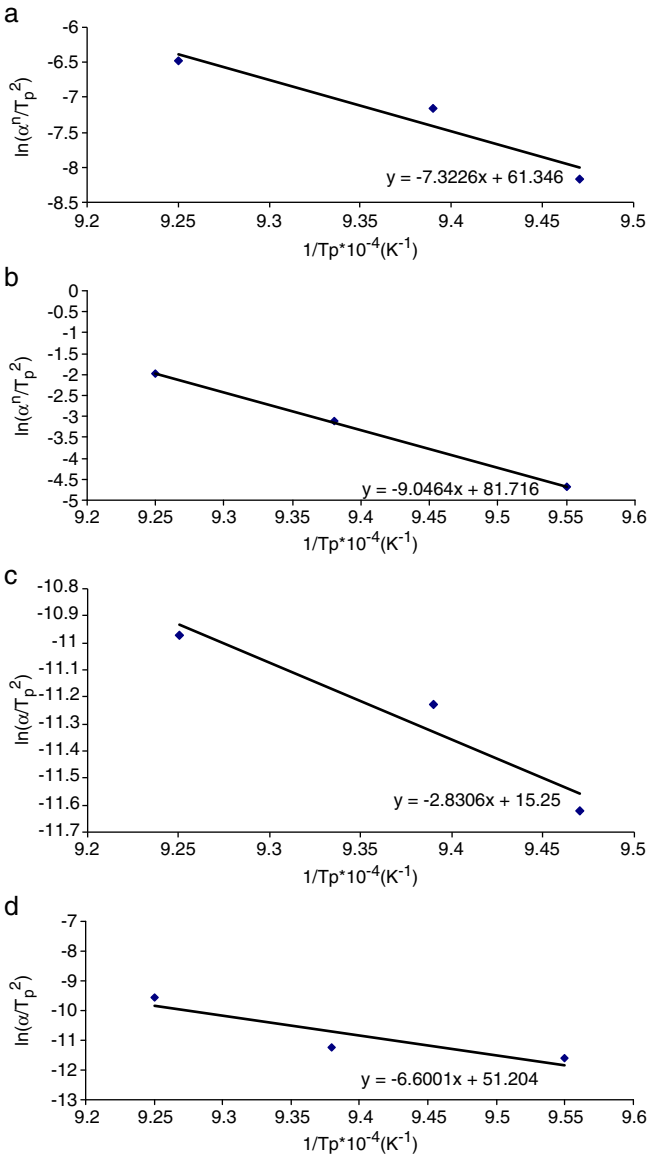

Figure 5. Matusita-Sakka ((**a**) L_0, (**b**) L_0MgF_6) and Kissinger ((**c**) L_0 and (**d**) L_0MgF_6) plots.

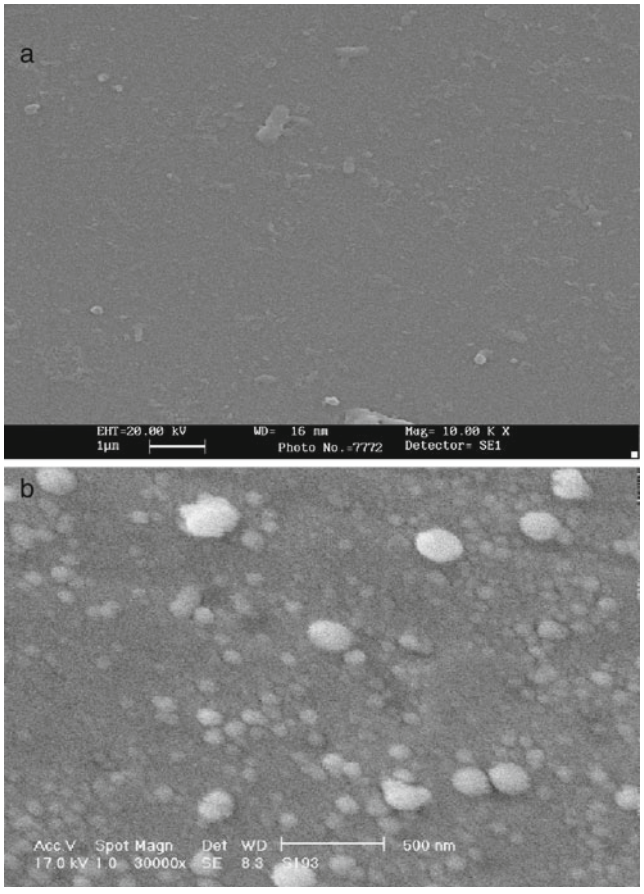

Figure 6. SEM photographs of polished and chemically etched surfaces of parent glasses: (**a**) L_0 and (**b**) L_0MgF_6.

2008). The graphical representation of the volume fraction crystallized for the exothermic curve shows typical sigmoid curve as a function of temperature for different heating rates.

Figure 4 shows plots of $\ln[-\ln(1-x)]$ vs $\ln\alpha$ for L_0 and L_0MgF_6 samples and the values of n were determined from the slopes of these plots. The values of n are found to be 2·5 and 4·68 (within the $\pm$ 0·2 error) for the first peak in L_0 and L_0MgF_6, respectively. These values indicate that bulk crystallizations have taken place in L_0 and L_0MgF_6. The m value for L_0 and L_0MgF_6 should be equal to $n-1$. When $m = 1{\cdot}5$, it implies that a transformation with two-dimensional growth by diffusion has taken place, but when $m = 3{\cdot}68$, it implies that a transformation with three-dimensional growth controlled by diffusion has taken place. From the above equation, the Avrami exponent (n) increased with addition of MgF_2 in base glass. The value was 4·68, in L_0MgF_6, indicating that crystallization of the glass–ceramics was largely homogenous and assuming a three-dimensional growth by diffusion.

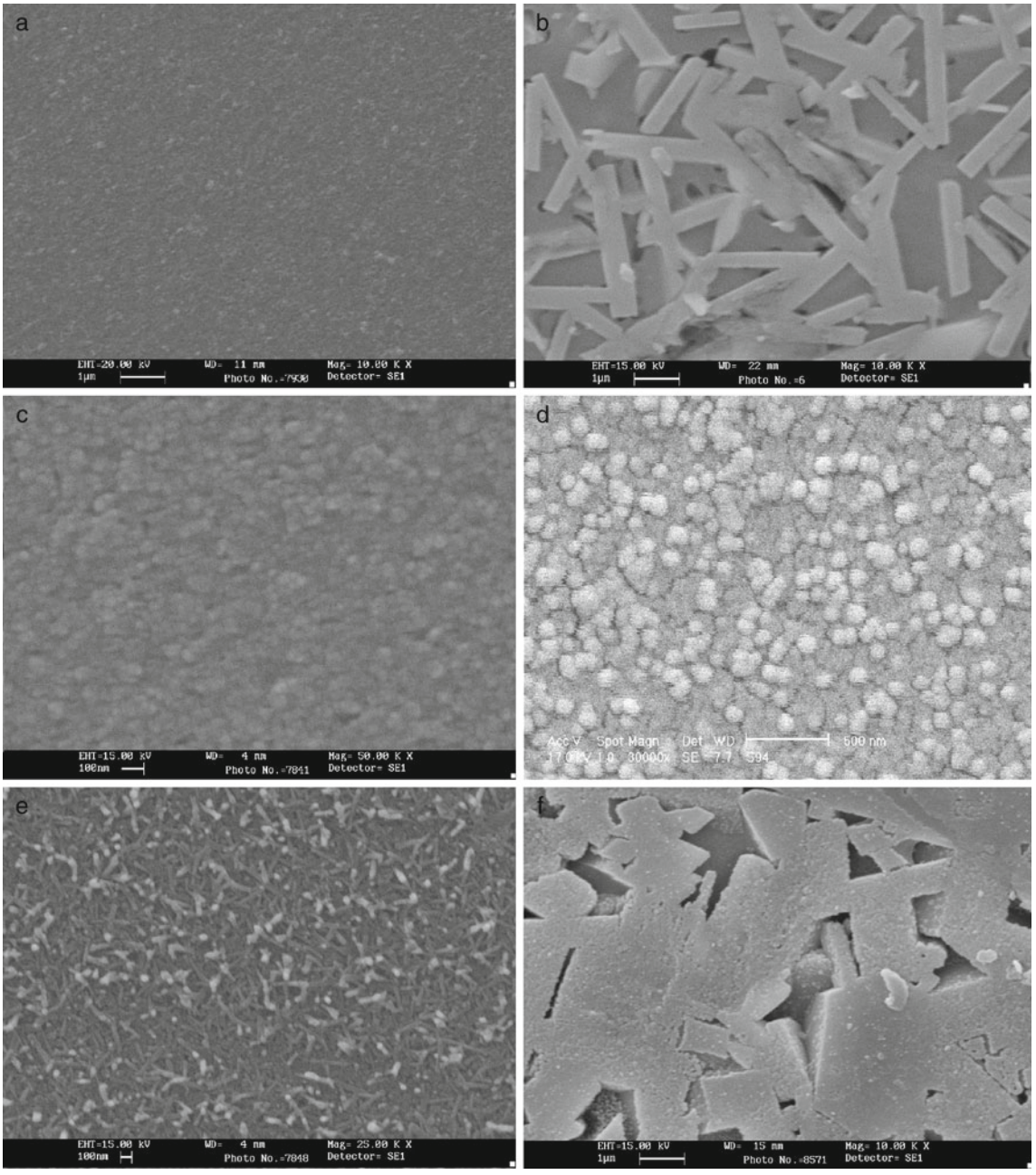

Figure 7. SEM photographs of polished and chemically etched surfaces of L_0 specimen heated at (**a**) 775°C for 2 h and (**b**) 1100°C for 2 h, L_0MgF_2 specimen heated at (**c**) 763°C, L_0MgF_4 specimen heated at (**d**) 810°C for 2 h and L_0MgF_6 specimen heated at (**e**) 795°C for 2 h and 1100°C for 2 h (**f**).

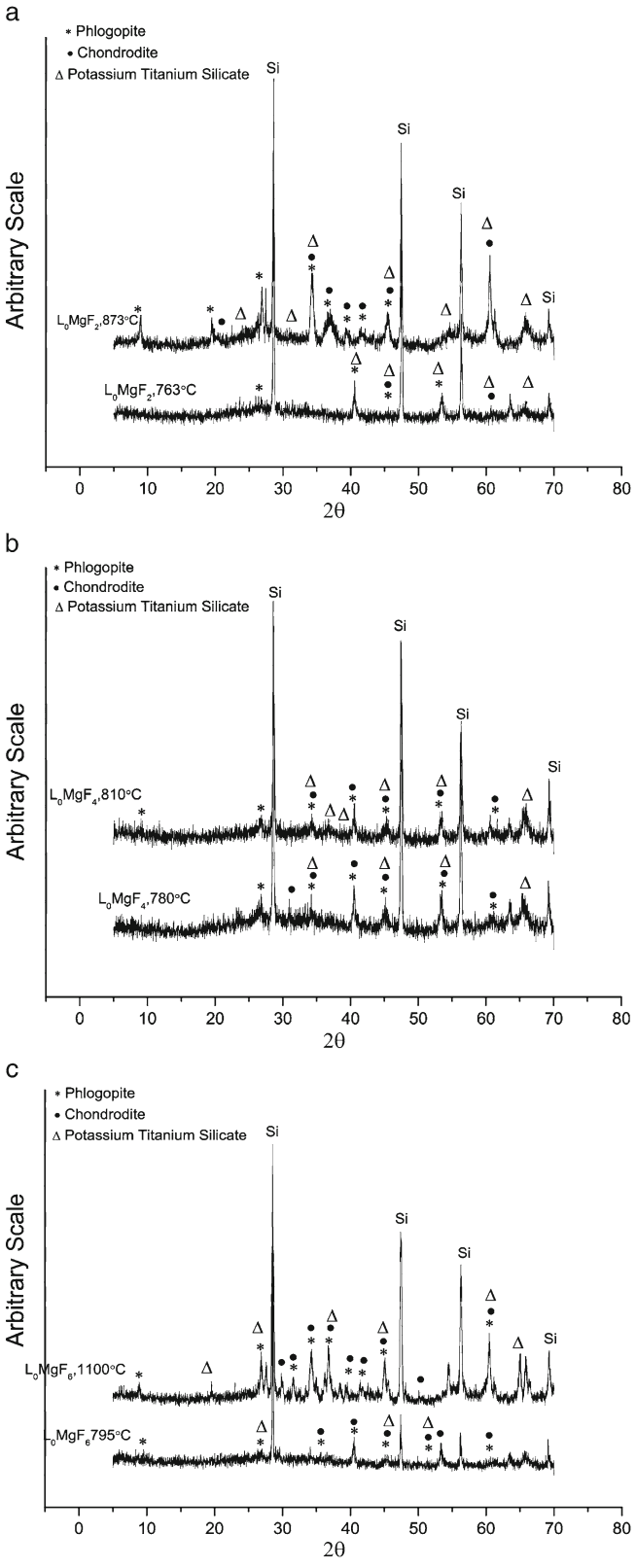

Figure 8. XRD patterns of (**a**) L_0MgF_2, (**b**) L_0MgF_4 and (**c**) L_0MgF_6.

Table 2. List of JCPDS files used to identify main crystal phase formed at different temperatures.

Crystal phase	JCPDS reference file
Potassium titanium silicate	01–077–1182
Chondrodite	00–014–0010
Phlogopite	00–034–0158

Table 3. Properties of glass sample reheated at 1000°C and 1100°C for 2 h.

Sample	Reheating temperature (°C)	H_v(GPa)	$\mu^1(J/mm^{-3})$	m
L_0	1000	2	4·7	0·39
L_0	1100	1·7	3·29	0·43
L_0MgF_6	1000	1·8	3·75	0·42
L_0MgF_6	1100	1·3	1·8	0·48

Figure 5 shows Matusita-Sakka and Kissinger curves for the estimation of E. The E_c values were obtained from the slopes of $\ln\left(\alpha^n/T_p^2\right)$ vs $1/T_p$ plots which were 405·72 ± 10 kJ/mol for L_0 and 752 ± 10 kJ/mol for L_0MgF_6 samples. On the other hand, using the Kissinger model (3), E_{ck} values of as-quenched glasses can be determined from the slope of the plots $\ln\left(\alpha/T_p^2\right)$ vs $1/T_pE_{ck}$ which was equal to 235·2 kJ/mol for L_0 and L_0MgF_6 and E_{ck} value was equal to 548 kJ/mol. These values are lower than the E_c values determined from the Matusita–Sakka model. Besides, the activation energy for the first peak in L_0 sample is lower than the activation energy for the peak in L_0MgF_6 sample.

3.4 *Crystallization mechanism*

Compared with K^+, Mg^{2+} has higher cationic field strength; usually the addition of MgF_2 tends to phase separation, improving the nucleation and crystallization of glass. It is generally accepted (Abdel-Hameed *et al* 2005) that fluorides are immiscible in silicate melts leading to glass in glass phase separation by which numerous droplets of one glass are formed and dispersed in another one. The microstructure of the investigated annealed glasses clearly featured liquid–liquid phase separation, as shown in (figure 6). In the case of L_0, round particles were embedded in glassy matrix (figure 6a). It has been reported that in mica glasses, droplets enriched in Mg, K and F can precipitate in silicate matrix phase (Abdel-Hameed *et al* 2005). The microstructure of L_0MgF_6 comprises numerous small spherical droplets distributed in glass matrix (figure 6b). Increasing the amount of MgF_2 resulted in more intense phase separation. As it has been shown in figure 7a, fine particles were observed at 775°C. Mica should be included in such fine particles

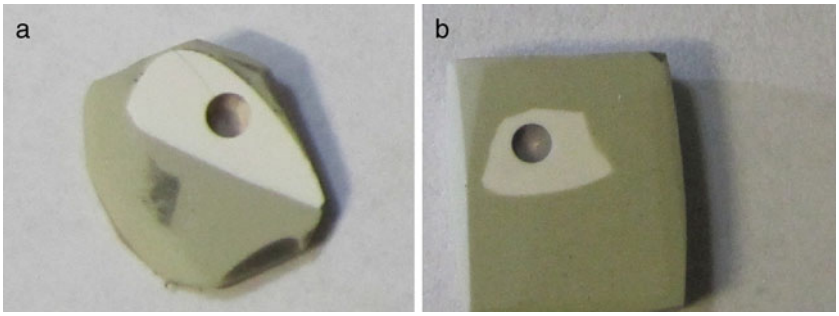

Figure 9. Photograph of drilling test for (**a**) L_0 specimen heated at 1100°C and (**b**) L_0MgF_6 specimen heated at 1100°C.

because it was already observed in the XRD pattern of samples heat treated at 775°C. At 1100°C, plate-like mica appeared (figure 7b). At this temperature, due to the growth at mica a complete interlocking microstructure is formed. The fine quasi-spherical particles were observed at 763°C in L_0MgF_2 (figure 7c). Fine spherical particles with nano size were precipitated at 810°C in the L_0MgF_4 (figure 7d). The observed particles in L_0MgF_2 and L_0MgF_4 correspond to the mica crystals which were observed in XRD patterns shown in figures 8a, b. At 795°C, plate-like mica appeared in L_0MgF_6 (figure 7e). Typically 'house card' structure of randomly oriented interlocked mica crystals was observed in L_0MgF_6 crystallized at 1100°C for 2 h (figure 7f).

3.5 *XRD analysis*

The JCPDS reference files used to identify various crystal phases formed are presented in table 2. Figure 8 shows XRD patterns of the samples. In the L_0 sample, major phases were phlogopite, potassium titanium silicate and chondrodite. It seems to us that the addition of MgF_2 increased the precipitation of phlogopite, which is beneficial to machinability of specimens. Besides phlogopite, chondrodite and potassium titanium silicate are also observed in L_0MgF_2, L_0MgF_4 and L_0MgF_6 glass–ceramic samples.

3.6 *Mechanical properties*

Table 3 shows machinability of the samples reheated at 1000°C and 1100°C for 2 h. According to table 3, L_0MgF_6 has the lowest H_v value after reheated at 1100°C for 2 h and it has the highest machinability parameter (m), indicating that L_0MgF_6 has good machinability. As the reheating temperature was increased, microhardness of glass–ceramic decreased. The calculated results of cutting energy (μ^1) and machinability parameter (m) are also listed in table 2. The lower the μ^1 value the better the machinability. Higher machinability parameter (m) values and lower cutting energy, μ^1 values, also indicate a highly machinable microstructure, which is beneficial to machineability of specimens (figures 9a, b).

4. Conclusions

Based on the obtained data, the activation energy 'E' estimated by Kissinger and Matusita–Sakka methods were different, but thier changes were similar. The activation energies for crystal growth were found to be in the range of 235–405 kJ/mol and 548–752 kJ/mol for the base glasses and samples with MgF_2, respectively. From microstructural point of view, the increase in crystallization temperature was found to be useful for the increase of aspect ratio of mica phase, which contributes for the machinability of the glass–ceramics. The changes in microhardness (H_v), cutting energy (μ^1) and machinability parameter (m) were related to the process parmeters and composition and were justified for estimating the machinability of glass–ceramics.

References

Abdel-Hameed S A M, Ghoniem N A, Saad E A and Margha F H 2005 *Ceram. Int.* **31** 499
Arora A, Shaaban E R, Singh K and Pandey O P 2008 *J. Non-Cryst. Solids* **355** 23
Baik D S, No K S, Chun J S and Cho H Y 1997 *J. Mater. Proc. Technol.* **67** 50
Boccaccini A R 1997 *J. Mater. Proc. Technol.* **65** 302
Greene K, Pomeroy M J, Hampshire S and Hill R 2003 *J. Non-Cryst. Solids* **325** 193
Kissinger H E 1957 *Anal. Chem.* **29** 1702
Likitvanichkul S and Lacourse W C 1995 *J. Mater. Sci.* **30** 6151
Matusita K and Sakka S 1980 *J. Non-Cryst. Solids* **38/39** 741
Ozawa T 1971 *Polymer* **12** 150
Radonjic Lj and Nikolic Lj 1991 *J. Eur. Ceram. Soc.* **7** 11
Riello P, Canto P, Comelato N, Polizzi S, Verita M and Hopfe S 2001 *J. Non-Cryst. Solids* **288** 127
Taruta S, Mukoyama K, Suzuki S S, Kitajima K and Takusayawa N 2001 *J. Non-Cryst. Solids* **296** 201
Wang P, Yu L, Xiao H, Cheng Y and Lian S 2009 *Ceram. Int.* **35** 2633